Received: 15 December 2021 | Revised: 1 June 2022 | Accepted: 14 June 2022

DOI: 10.1111/cas.15470

ORIGINAL ARTICLE

Cancer Science WILEY

Silybin suppresses ovarian cancer cell proliferation by inhibiting isocitrate dehydrogenase 1 activity

Zibo Wei[1] | Shuangyan Ye[2] | Haipeng Feng[3] | Chong Zeng[1] | Xinhuai Dong[1] | Xiaokang Zeng[1] | Liming Zeng[1] | Xu Lin[1] | Qiuzhen Liu[1] | Jie Yao[1,4]

[1]Medical Research Center, Shunde Hospital, Southern Medical University (The First People's Hospital of Shunde), Foshan, China

[2]Medical Research Center, The Eighth Affiliated Hospital, Sun Yat-Sen University, Shenzhen, China

[3]Department of Pathology, Shunde Hospital, Southern Medical University (The First People's Hospital of Shunde), Foshan, China

[4]Department of Laboratory Medicine, Shunde Hospital, Southern Medical University (The First People's Hospital of Shunde), Foshan, China

Correspondence
Qiuzhen Liu and Jie Yao, Department of Laboratory Medicine and Medical Research Center, Shunde Hospital, Southern Medical University (The First People's Hospital of Shunde, Foshan), No. 1, Jiazi Road, Shunde District, Foshan, Guangdong 528308, China.
Email: liuqiuzhen@126.com and jie.yao413@yahoo.com

Funding information
This study was supported by the National Natural Scientific Foundation of China (81770148); Guangdong Medical Research Foundation (A2022159); The Scientific Research Start Plan of Shunde Hospital, Southern Medical University (YNZX0002,YNZX0003, SRSP2019002, SRSP2019003); Shunde Hospital of Southern Medical University (2019014) for support.

Abstract

Metabolic reprogramming is a sign of malignant tumors, and targeting the metabolism of tumor cells has become a promising therapeutic approach. Here, we report that Silybin (a nontoxic flavonoid commonly used for liver protection) exhibits prominent anti-tumor effects on human ovarian cancer cells. Treatment of an ovarian cancer cell line with Silybin interfered with glutamine metabolism and the tricarboxylic acid cycle. We applied the drug affinity responsive target stability approach to show that Silybin binds to isocitrate dehydrogenase 1 (IDH1). This combination leads to reduced phosphorylation of IDH1 and inhibits enzyme activity. IDH1 dysfunction significantly increases the ratio of NADP/NADPH in the cell, causing an increase in reactive oxygen species generation. Immunohistochemistry demonstrated that IDH1 was increased in ovarian cancer samples compared with normal para-tumoral tissues. Xenograft murine experiments indicated that Silybin administered orally suppressed the growth of the tumor formed by ovarian cancer cells. In combination, our data strongly suggest that Silybin targets IDH1 in ovarian cancer cells and may be a novel treatment candidate.

KEYWORDS
cancer plasticity, energy metabolism reprogramming, ovarian cancer, redox homeostasis, tumor microenvironment

Abbreviations: D-2HG, D-2-hydroxyglutarate; DARTS, drug affinity responsive target stability; ECAR, extracellular acidification rate; GSH, reduced glutathione; GSSG, oxidized glutathione disulfide; IDH1, isocitrate dehydrogenase; M5, five ^{13}C atoms; NAC, *N*-acetylcysteine; OCR, oxygen consumption rate; OV, ovarian cancer; PPP, pentose phosphate pathway; ROS, reactive oxygen species; SIL, Silybin; TCA, tricarboxylic acid; α-KG, α-ketoglutarate.

Zibo Wei, Shuangyan Ye, and Haipeng Feng contributed equally to this work.

1 | INTRODUCTION

Ovarian cancer is a highly malignant tumor from which more than 0.125 million women die every year.[1] The cancer can become resistant to chemotherapy and radiotherapy, resulting in treatment failure.[2] To overcome this, alternative treatment strategies are urgently needed, in addition to the identification of new biomarkers.

Silymarin contains four components. The main active component is SIL, which is present together with isosilibinin, silydianin, and silychristin.[3–5] SIL (also written as silibinin) has been approved by the United States Food and Drug Administration to treat liver diseases.[6] Recently, it was found that SIL has anti-cancer activity, as demonstrated for prostate and colorectal cancers.[7] SIL was also shown to reduce the glycolytic activity of pancreatic ductal adenocarcinoma cells, which was correlated to reduced the expression of glycolytic enzymes GLUT1 and HKII. It has also been reported that SIL treatment could increase apoptosis in human ovarian cancer cells.[8] Consistent with a previous study, we also observed that apoptosis increased following a 24 h treatment with 50 μM SIL, but no changes were observed with twice that dose, although cellular morphological changes were observed. However, the biochemical role of SIL associated with cellular metabolism in ovarian cancer remains unexplored to date.

Tumor cells enhance the expression of antioxidant components that are expressed to detoxify increased ROS levels and restore a redox balance, while maintaining protumorigenic signaling. Therefore, altering ROS production may provide a potentially effective therapeutic strategy for cancer.[9] Although SIL participates in multiple cellular processes, there is some controversy about its role in ROS production. It was shown that SIL treatment led to increases in ROS generation and downregulation of the MAPK/ERK and Akt pathways.[8] Studies on isolated mitochondria from liver cells revealed that SIL reduced ROS production associated with electron transfer chain activity.[10] IDH is a key enzyme of the TCA (citric acid) cycle. In humans, five IDH genes exists that code for three distinct IDH enzymes: IDH1, IDH2, and IDH3. The activity of IDH1 and IDH2 depends on nicotinamide adenine dinucleotide phosphate ($NADP^+$), whereas that of IDH3 is nicotinamide adenine dinucleotide (NAD^+) dependent.[11] Several mutations in the IDH genes are involved in oncogenesis, such as the R132H mutation in IDH1. This mutation results in novel enzymatic activity that catalyzes the NADPH-dependent reduction of alpha-ketoglutarate (α-KG) to D-2-hydroxyglutarate, as has been demonstrated in various forms of cancer.[12,13] IDH1 is overexpressed in glioblastoma cells, which facilitate tumor cell growth in vitro and in vivo and decreases the survival of glioblastoma patient-derived xenografts.[14] A recent study demonstrated that suppression of IDH1 activity reduced tumor cell growth through an effect on redox homeostasis.[14]

In this study, we focused on the function of SIL in vitro and in vivo, and explored its underlying regulatory mechanisms. For in vitro experiments, two ovarian cancer cell lines were used, and in vivo experiments involved a xenograft mouse model. We confirmed high levels of IDH1 expression in ovarian cancer tissues obtained from patients and found that SIL resulted in a reduction of the level of IDH1 phosphorylation, interfered with the TCA cycle and increased the production of ROS, resulting in tumor cell death.

2 | MATERIALS AND METHODS

2.1 | Study approval

The Ethics Committee of Shunde Hospital (FoShan) approved the use of discarded tissue from patients with ovarian cancer. Informed consent for the procurement and analysis of these samples was also obtained.

2.2 | Chemicals and reagents

SIL was purchased from Cayman Chemical Company (Michigan, USA), and radiolabeled [^{13}C-U_6] glucose and [^{13}C-U_5] glutamine were obtained from Cambridge Isotope Laboratories Inc. (Boston, MA, USA). Glucose-free DMEM and glutamine-free RPMI-1640 medium were purchased from Gibco (Waltham, MA, USA). The primary antibody against IDH1 was rabbit polyclonal ab172964 (Abcam, Cambridge, MA, USA). Glucose, oligomycin, 2-deoxyglucose (2-DG), carbonyl cyanide 4-(trifluoromethoxy)phenylhydrazone (FCCP), and rotenone–antimycin A were purchased from Agilent (Agilent Technologies, Santa Clara, CA, USA). NAC was purchased from the Beyotime Institute of Biotechnology (Shanghai, China).

2.3 | Cell culture

Human ovarian cancer cell lines OVCAR3 and SKOV3 were obtained from the Southern Medical University Cancer Institute (Guangzhou, China). All experiments were performed with mycoplasma-free cells. The cells were cultured in RPMI 1640 supplemented with 10% fetal bovine serum and 1% penicillin/streptomycin in a humidified 37°C incubator.

2.4 | Cell transfection

shRNA-IDH1 was procured from WZ Biosciences Inc. for gene silencing. Compounds were inserted into the lentiviral pLenti-U6-CMV-copGFP-P2A-Puro vector. The full-length *IDH1* gene was inserted into the lentiviral pLenti-EF1a-FH-CMV-RFP-P2A-Puro vector. Both vectors were introduced into OVCAR3 cells, and puromycin was applied to screen for stable cell clones.

2.5 | Patient samples

The 27 pairs of cancerous tissues and adjacent normal tissues used in this study were collected from the Department of Pathology, Shunde Hospital, Southern Medical University (The First People's

Hospital of Shunde, Foshan). The study was conducted in accordance with the Declaration of Helsinki (as revised in 2013) and approved by the ethics board of Shunde Hospital, Southern Medical University. All participants were counseled regarding the potential uses of their tissue and had given their written consent.

2.6 | Determination of enzyme activity and cell apoptosis

The ratios of $NADP^+$/NADPH and of glutathione/glutathione disulfide (GSH/GSSG) were determined with dedicated kits (Beyotime Institute of Biotechnology, Shanghai, China). IDH1 activity was detected using recombinant human IDH1 (Abcam, Cambridge, UK) and an IDH activity colorimetric assay kit (BioVision, San Francisco, CA, USA). Cell apoptosis was determined using a TUNEL apoptosis detection kit (YEASEN, Shanghai, China).

2.7 | Cytotoxicity assays

CCK-8 assays were performed to determine the viability of the OVCAR3 cells following SIL treatment. The cells were seeded onto 96-well plates, and grown for 24 h, and subsequently exposed to SIL at different concentrations, with a negative control included. The cells were cultured for 24 h in an incubator, after which 10 μl CCK-8 was added to every well and cells cultured at room temperature for a further 2 h. Absorbance was then measured using a Bio-Tek multimode reader. The experiment was performed in triplicate.

2.8 | Immunoblotting

Cells were washed twice with 2 ml PBS, after which they were lysed with RIPA lysis buffer containing 1% protein phosphatase inhibitors and 1% PMSF (Fdbio Science, Hangzhou, China). The protein concentration in the sample was determined using a BCA kit (Beyotime, Shanghai, China) with reference to a standard curve. The samples were mixed with SDS-PAGE loading buffer containing DTT (Solarbio, Beijing, China) and, after separation, the bands were transferred electrophoretically onto PVDF membranes (Millipore, USA). The PVDF membranes were blocked with 5% bovine serum albumin for 1 h. Incubation was carried out with the following primary antibodies: anti-IDH1 antibody (Abcam, catalog no. ab172964, 1:5000 dilution), anti-tubulin antibody (Affinity, catalog no. AF7011, 1:1000 dilution), anti-P(S-T-Y) antibody (abmart, catalog no. M210030, 1:2000 dilution), anti-ERK antibody (Bioss, catalog no. bsm52259R, 1:1000 dilution), anti-phospho-ERK antibody (Bioss, catalog no. bs3016R, 1:1000 dilution), anti-AKT antibody (Bioss, catalog no. bs6951R, 1:1000 dilution), and anti-phospho-ERK antibody (Bioss, catalog no. bs5193R, 1:1000 dilution). Membranes were washed with PBS three times and incubated with HRP-conjugated IgG secondary antibodies (Proteintech, catalog nos. 15015 and 15014, 1:5000 dilutions) for 1 h at room temperature. Signals were visualized using the ECL Western Blot Kit (Millipore, catalog no. P90720).

2.9 | Drug affinity responsive target stability (DARTS) analysis

The DARTS assay was performed according to a published protocol.[15] OVCAR3 cells were collected and grown to 80% confluency, washed with PBS, and lysed in M-PER (catalog 78501, Thermo Fisher Scientific) containing 1× protease phosphatase inhibitor cocktail (catalog P1048, Beyotime, Shanghai, China). The protein concentration after adding TNC buffer was measured using the BCA protein assay kit (catalog P0012s, Beyotime, Shanghai, China). The lysate was divided into two 1.5 ml tubes and incubated with DMSO or SIL for 1 h at room temperature. After incubation, the mixture was digested with pronase (catalog 10165921001, Roche) at 37°C for 1 h. Following SDS-PAGE, specific bands indicative of protection were excised and analyzed using LC–MS (Shenzhen Win innovate Bio).

2.10 | ROS level analysis

Intracellular ROS was detected using an oxidation-sensitive fluorescent probe (DCFH-DA) as described previously.[8] For dichlorofluorescein (DCF) fluorescence, a flow cytometer was used (BD, USA). For each sample 10,000 events were analyzed and the experiments were performed at least three times.

2.11 | Glucose consumption assay and lactate secretion assay

Cells were seeded into 96-well plates at a density of 6000 cells per well. After cells attached to the wells, the medium was exchanged for medium containing 100 μM SIL or not and cells were cultured for a further 24 h. Next, the culture medium was collected and the Glucose Colorimetric Assay Kit II (catalog no. K686-100, BioVision) was used for a glucose consumption assay according to the manufacturer's instruction. In addition, the Lactate Colorimetric Assay Kit II (catalog no. K627-100, BioVision) was used for a lactate secretion assay according to the manufacturer's instruction. Absorbance was measured at 450 nm on a microplate.

2.12 | Metabolic flux analysis (MFA) with stable isotope tracing

For in vitro studies, 5×10^5 cells/well OVCAR3 cells were seeded with basal medium and cultured for 12 h, after which the culture medium was changed to glutamine-free RPMI 1640 medium containing [U-$^{13}C_5$]glutamine. Glutamine was added to the cells at indicated time points at a final concentration of 2 mM. The cells

were washed with PBS and lysed directly in extraction buffer, frozen in liquid nitrogen and stored at −80°C. After 1 min, 200 µl of ice-cold norvaline (5 µg/ml) was added to each well and the content was collected in tubes. In total, 500 µl of cooled chloroform was added and fully mixed. Samples were immediately centrifuged at 13,000 ***g*** for 10 min at 4°C to separate the phases and the chloroform phase was extracted and dried using an airflow. The extract was then either used directly for derivation or stored at −20°C. Derivation was performed within a day, as described previously.[16] Metabolites were profiled using GC–MS comprised of a Thermo GC 1300 gas chromatograph connected to a Thermo MS ISQ spectrometer.

2.13 | Mitochondrial respiration

The oxygen consumption rate and extracellular acidification rate (ECAR) in the cultured cells were detected using an XF96 Extracellular Flow analyzer (Seahorse Bioscience, Billerica, MA, USA), according to the manufacturer's protocols and previous descriptions.[16] The concentrations of compounds injected during the analysis were 10 mM glucose, 1 µM oligomycin, 50 mM 2-DG and 1 µM oligomycin, 0.5 µM FCCP, and 0.5 µM rotenone–antimycin A for the cells. Data were obtained using XF96 Analyzer software.

2.14 | Immunohistochemistry

Paraffin-embedded tumor blocks and sections were stained with H&E using standard methods. IDH1 immunohistochemistry was carried out according to the SP Rabbit & Mouse HRP Kit (DAB) using 1:200 rabbit polyclonal ab172964 as the primary antibody against IDH1.

2.15 | Phos-tag assay

Phos-tag analysis was performed according to the manufacturer's instructions (APExBIO, F4002). First, the proteins were separated onto 10% SDS polyacrylamide gels prepared with 50 µM phosbind acrylamide and 40 µM $ZnCl_2$. Second, the gel was equilibrated in a buffer containing 5 mM EDTA for 10 min before transfer. Finally, proteins were transferred onto a PVDF membrane for immunoblot analyses.

2.16 | Immunoprecipitation assay

Cells were lysed in lysis buffer (20 mM Tris–HCl [pH 7.9], 100 mM NaCl, 0.2% NP-40, 20% glycerol) containing 1% protein phosphatase inhibitors. The lysates were incubated with anti-IDH1 or anti-IgG primary antibody at 4°C overnight. Bound proteins were eluted with 0.1 M glycine (pH 2.5) and neutralized with 1 M Tris buffer. Eluted proteins were detected using western blot or used for IDH1 activity.

2.17 | Murine xenograft experiments

Female BALB/c nude mice (3–5 weeks old) were obtained from Beijing Hua Fu Kang Biotechnology Co. Ltd (Beijing, China). The animals were housed under 12 h light/dark cycles, at 26–28°C and a relative air humidity of 50%, and had free access to water and food. All animal experiments were performed in accordance with National Institutes of Health Guidelines for the Care and Use of Laboratory Animals, following a protocol approved by the Medical Ethics Committee of Shunde Hospital, Southern Medical University (The First People's Hospital of Shunde, Foshan). The mice were randomly divided into nine groups: NaCl and SIL; Sh-IDH1 + NaCl and Sh-IDH1 + SIL; OV-IDH1 + NaCl and OV-IDH1 + SIL; OV-IDH1, sh-IDH1, and NC; a sample size of eight animals per treatment group was chosen.

OVCAR3 cells (2×10^6) were injected subcutaneously into the right foreleg of each animal. At 10 days after this injection, SIL (100 mg/kg) or saline (control) was administered daily by oral gavage for a period of 6 weeks, after which the animals were sacrificed by cervical dislocation and the tumors were excised.

2.18 | Statistical analysis

Statistical analyses were performed using GraphPad Prism statistical software (GraphPad Software, Inc., San Diego, CA, USA). Statistical tests were undertaken using GraphPad Prism software. The number of biological replicates was presented by individual data points in each bar graph. The differences between groups were calculated using two-tailed Student's *t*-test or two-way ANOVA. Error bars represent SEM, and a *P*-value <0.05 was considered statistically significant. $^{*}P<0.05$, $^{**}P<0.01$, $^{***}P<0.001$.

3 | RESULTS

3.1 | SIL inhibits cell proliferation through increasing ROS levels

When cultured OVCAR3 cells were treated with SIL at 50 µM or 100 µM for 48 h, this led to increased apoptosis (Figure 1A). SIL treatment decreased cell viability at time points 24 h and 48 h, with both tested concentrations (Figure 1B). In subsequent experiments, cells were exposed to 100 µM SIL for 24 h. To determine whether SIL inhibited cell growth by interfering with redox homeostasis, changes in DCFH-DA were measured in treated OVACR3 cells, which demonstrated a significant increase in ROS generation. To determine whether ROS affects cell proliferation and morphology, rescue experiments using antioxidants (NAC) were

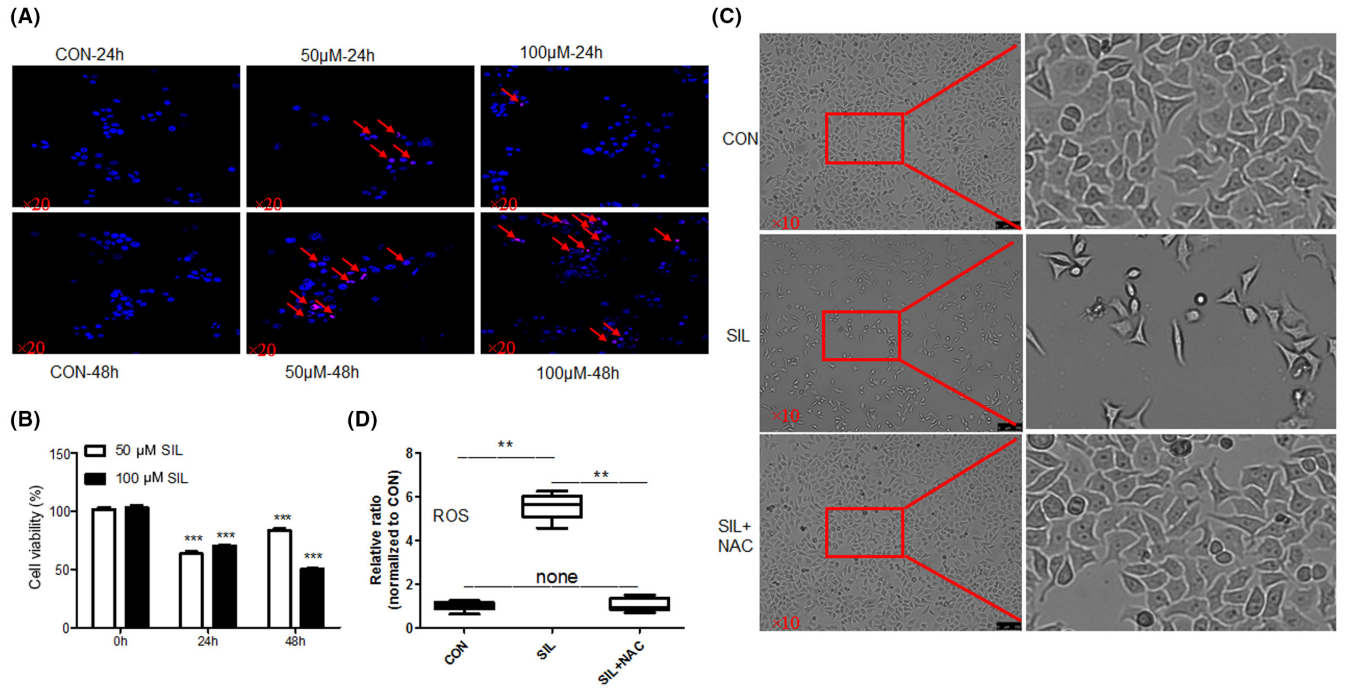

FIGURE 1 SIL inhibits cell proliferation through increasing ROS levels. (A) OVCAR3 cells were cultured in the desired concentrations of SIL (0, 50, 100 μM) for 24 h, 48 h individually and subjected to fluorescence microscopy. Blue fluorescence indicates the nucleus and red arrows indicate the apoptotic site. (B) The viability of OVCAR3 cells after incubated at different concentrations of SIL (0, 50, 100 μM) for 24 h, 48 h and subjected to CCK-8 assay. Bars represent the means ± SD of three independent experiments. (C) OVCAR3 cells were exposed to 100 μM SIL in the presence or absence of 5 mM NAC for 24 h and morphological changes were observed. Magnification is ×10. (D) OVCAR3 cells were loaded with DCFH-DA for 1 h and afterwards exposed to 100 μM SIL in the presence or absence of 5 mM NAC for 24 h. DCF fluorescence intensity was measured by flow cytometry. Statistical analysis: Student's *t*-test. Error bars represent SEM. A *P*-value <0.05 was considered statistically significant. $^{**}P<0.01$, $^{***}P<0.001$, All experiments were repeated three times

performed (Figure 1C,D). These results indicated that SIL inhibits cell proliferation and induces morphological change through increasing ROS levels.

3.2 | SIL inhibits mitochondrial oxidative phosphorylation and PPP

To investigate whether SIL treatment affected energy generation in the cell, we evaluated the oxygen consumption rate in treated OVCAR3 cells in the presence of specific inhibitors. Oligomycin, an ATP synthase inhibitor, inhibits oxidative phosphorylation. The experiments showed that basal respiration, maximal respiration, and ATP production were all reduced in OVCAR3 cells following SIL treatment (Figure 2A,B,E). The extracellular acidification rate (ECAR) was measured as the basal acidification rate before the addition of glucose, which determines glycolysis-dependent ECAR. Oligomycin was added to measure glycolytic capacity, whereas 2-DG was added to inhibit glycolysis and determine nonglycolytic acidification. The tested cell energy metabolism indicated that ECAR was not affected by SIL treatment (Figure 2C,D). There was no difference in the effect of SIL on glucose uptake and lactate production in OVCAR3 cells, which is an important indicator of glycolysis (Figure 2F). The total reaction formula of the pentose phosphate pathway (PPP) is:

$$\text{G-6-P} + 12\text{NADP}^+ + 7\text{H}_2\text{O} \rightarrow 6\text{CO}_2 + \text{Pi} + 12\text{NADPH} + 12\text{H}^+$$

PPP is an important donor of NADPH. The results showed that PPP is suppressed, the intracellular $NADP^+$ concentration increased and NADPH decreased after SIL treatment (Figure 2F).

3.3 | SIL suppresses the TCA cycle in OVCAR3 cells and accelerates glutamine reduction

To investigate the effect of SIL on glutamine metabolism, stable isotope-traced glutamine was used to analyze metabolic fluxes. As described by DeBerardinis and colleagues,[17] glutamine-derived reducing nitrogen is an important material for maintaining nucleotide and nonessential amino acids biosynthesis and also replenishes the TCA cycle intermediates. Moreover, glutamine catabolism is the main source of NADPH. This cofactor is essential for electron transfer and to maintain redox balance. SIL treatment increased the total levels of ^{13}C-labeled glutamine, glutamate, and citrate, and the Glu M5/Gln M5 ratio in the cells, indicating that it promotes the uptake of glutamine (Figure 3A,D,E). The α-KG derived from glutamate can enter oxidative metabolism, or form citrate with four ^{13}C atoms (M4) from the reductive carboxylation of α-KG with five (M5) C atoms.

Glutamate can enter the TCA cycle, which converts it to M4 succinate, M4 malate, and then M4 citrate. Our results showed

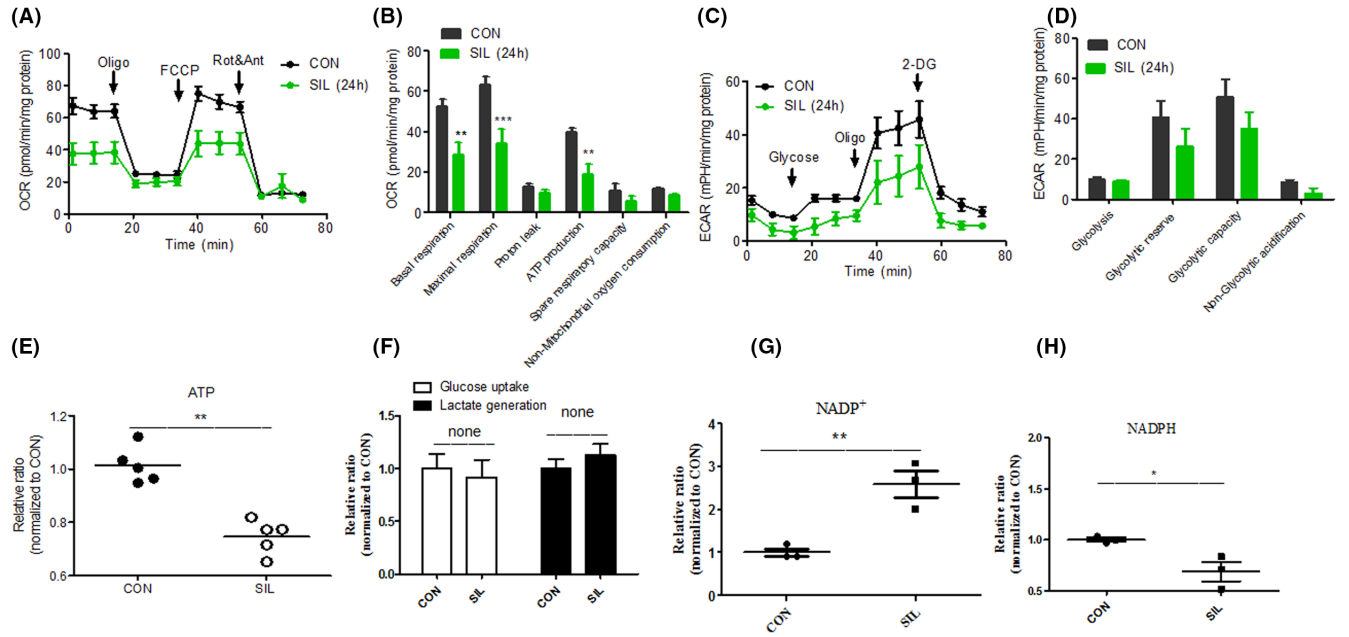

FIGURE 2 SIL inhibits mitochondrial oxidative phosphorylation and PPP. (A, B) Detection of OCR using Seahorse XF technology in OVCARs cells after treatment with 100 μM SIL for 24 h. Each value represents the mean ± SD in three independent experiments. (C, D) Detection of cellular ECAR using Seahorse XF technology in OVCARs cells after treatment with 100 μM SIL for 24 h. Statistical analysis: Student's *t*-test was used in and two-way ANOVA was used in. (E) ATP content in OVCARs cells after treating with 100 μM SIL for 24 h. (F) Glucose uptake and lactate production of the OVCAR3 cells. (G, H) Content of the $NADP^+$ and NADPH for the OVCAR3 cells. Error bars represent SEM, and $P < 0.05$ was considered statistically significant. $^*P < 0.05$, $^{**}P < 0.01$, $^{***}P < 0.001$, All experiments were repeated three times

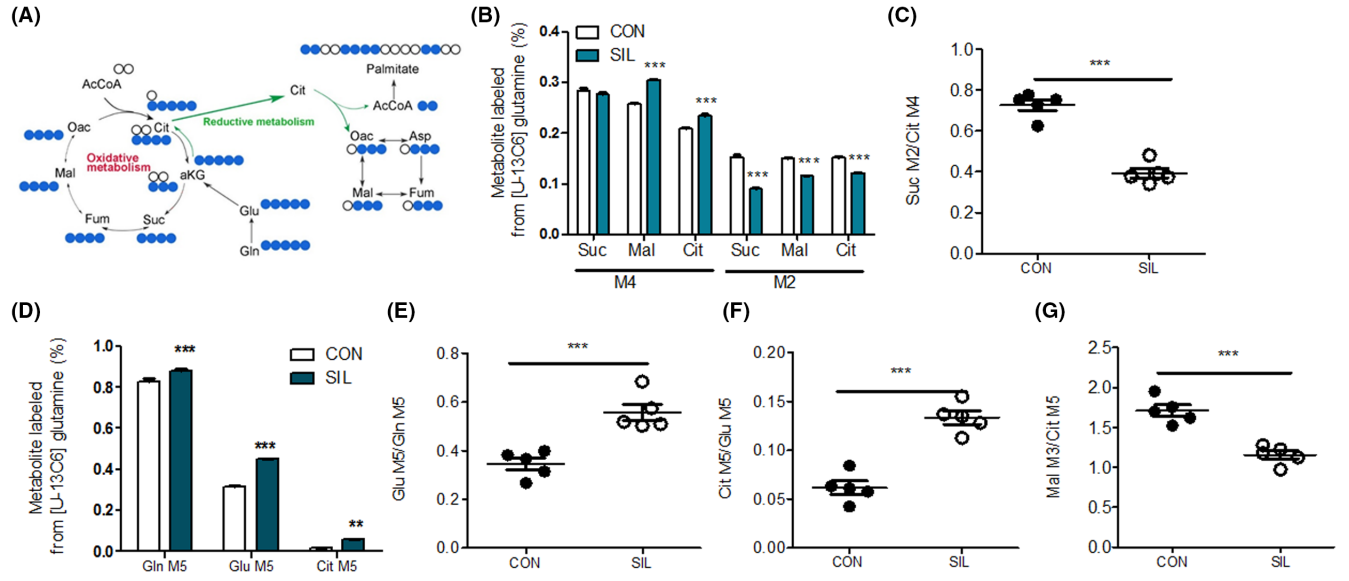

FIGURE 3 SIL suppresses the TCA cycle in OVCAR3 cells and accelerates glutamine reduction. (A) Schematic of carbon atom (circles) transitions and tracers used to detect glutamine metabolism. (B) Relative level of oxidative glutamine metabolism, determined by M4 and M2 labeling TCA cycle metabolites from [U-13C5] glutamine. Succinic (Suc), malate (Mal), and citrate (Cit). (C, E–G) Ratios of, Suc M2/Cit M4, Glu M5/Gln M5, Cit M5/Glu M5 and Mal M3/Cit M5. (D) Relative level of M5 glutamine (Gln), glutamate (Glu), and citrate (Cit) from [U-13C5] glutamine after 100 μM SIL treatment or not for 24 h. The ratios of Glu M5/Gln M5. Statistical analysis: Student's *t*-test was used in (C, E–G) and two-way ANOVA was used in (B, D). Error bars represent SEM, and a *P*-value <0.05 was considered statistically significant. $^{**}P < 0.01$, $^{***}P < 0.001$, All experiments were repeated three times

that SIL induced an increase in the M5 glutamine-derived oxidative intermediates M4 malate and M4 citrate, but it reduced levels of M2 succinate, M2 malate, and M2 citrate, all derivatives from M4 citrate (Figure 3B). We used product/substrate ratios to indicate the metabolic flow. This demonstrated that the ratio of M2 succinate/M4 citrate, and that of M3 malate/M5 citrate were both reduced,

indicating that SIL inhibits the TCA cycle (Figure 3C,G). The ratio M5 citrate/M5 glutamate was increased, which indicates that SIL promotes glutamine reductive carboxylation (Figure 3F).

3.4 | IDH1 as the target enzyme for SIL and its expression patterns in patient specimens

To further elucidate the mechanism by which SIL affected increased glutamine reduction, we applied DARTS, an approved method to screen or verify drug–protein binding. The subsequent SDS-PAGE gel revealed a strong protein band at 45 kDa that had been protected in the proteolyzed extracts of SIL-treated cells. This protein band was excised and, together with the band from the control lane, these were examined by mass spectrometry, and results showed that there were 128 differential proteins (Table S1). Based on metabolomic analysis, there are five metabolic enzymes that may be target molecules (Table S1). Combined with the two above results, we then confirmed the interaction of SIL protein with western blot experiments, which ultimately identified IDH1 as the target protein of SIL (Figures 4B and S1). Immunohistochemical and H&E analysis of clinical ovarian cancer samples were then performed. H&E staining revealed increased sizes of nucleoli and nuclear abnormalities compared with the para-carcinoma tissue. Immunohistochemistry showed that clinical carcinoma tissues expressed higher levels of IDH1, P53, CEA, CK7, and Ki-67 than para-carcinoma tissue (Figure 4C–F).

3.5 | SIL inhibit the activity of IDH1 by dephosphorylation

Western blotting was performed to confirm whether SIL inhibited the conversion of α-KG to isocitrate by suppressed IDH1 phosphorylation. The results showed that SIL treatment did not change IDH1 expression, but reduced its total level of phosphorylation (Figure 5A,E). To find direct evidence of phosphorylation of IDH1, we utilized IDH1 antibody to pull down IDH1 protein, using a pan-phosphorylated antibody P-(S-T-Y) that can detect the change in serine, threonine, and tyrosine phosphorylation levels. The experimental results demonstrated that there was no change in the total protein in the cell, but reduced IDH1 levels of phosphorylation (Figure 5B,E). We confirmed that cells expressed wild-type IDH1, independently of DMSO or SIL treatment (Figure 5C,F). The activity of purified recombinant IDH1 protein was inhibited by SIL treatment (Figure 5D,G). SIL also inhibited IDH activity in cells (Figure S2).

3.6 | Effect of SIL on the ERK and Akt

The level of IDH1 was suppressed by the addition of IDH1-IN-1 (a specific inhibitor for IDH1) (Figure 6A). In addition, to ascertain whether SIL downregulated ERK and Akt, western blot analysis was carried out using antibodies specific for their respective phosphorylated form. Phosphorylation of ERK and Akt was reduced (Figure 6B). This phenomenon was prevented by the addition of NAC (Figure 6C).

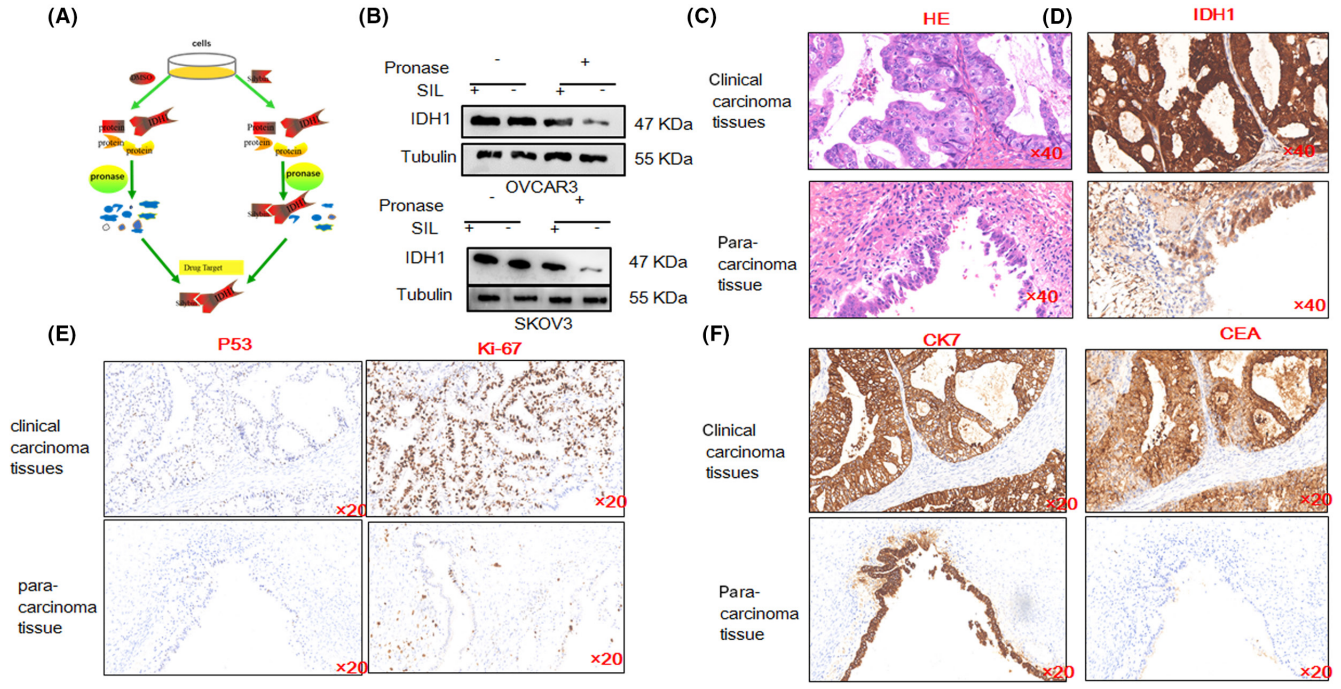

FIGURE 4 IDH1 as the target enzyme for SIL and its expression patterns in patient specimens. (A) Protein lysates were split into two and subjected to proteolysis. Less degraded proteins in the drug-treated cells were searched. (B) Drug affinity responsive target stability with SIL shows interaction with IDH1 from reduced degradation of IDH1. (C) H&E analysis of clinical ovarian cancer samples. (D–F) Immunohistochemical analysis of the pattern of IDH1, P53, CEA, CK7, and Ki-67 in primary tumor

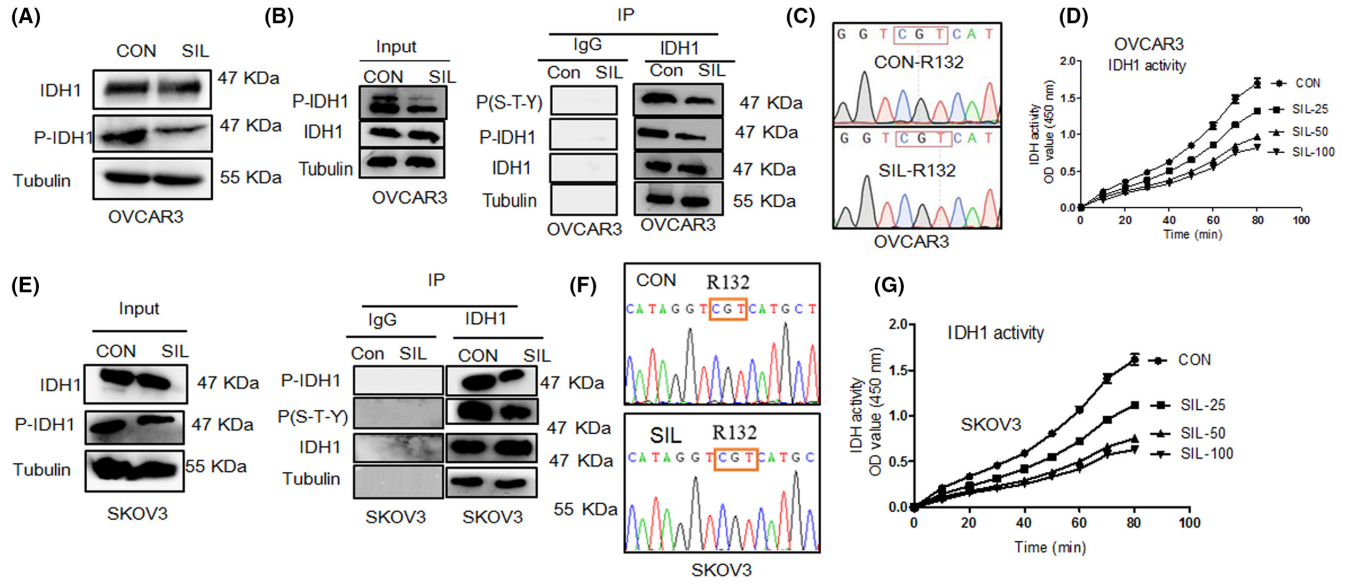

FIGURE 5 SIL inhibit the activity of IDH1 by dephosphorylation. (A) The effects of SIL on the phosphorylation of IDH1 were analyzed using a Phos-tag assay. (B, E) IDH1 proteins were purified using IDH1 antibody, and then, using pan-phosphorylated antibody P-(S-T-Y) and Phos-tag assay to detect the phosphorylation level using western blot. (C, F) DNA sequencing example of R132H not mutation in both control (CON) and SIL treatment IDH1. (D, G) Enzymatic activity of IDH1 treated with control and different concentrations SIL ($n = 5$)

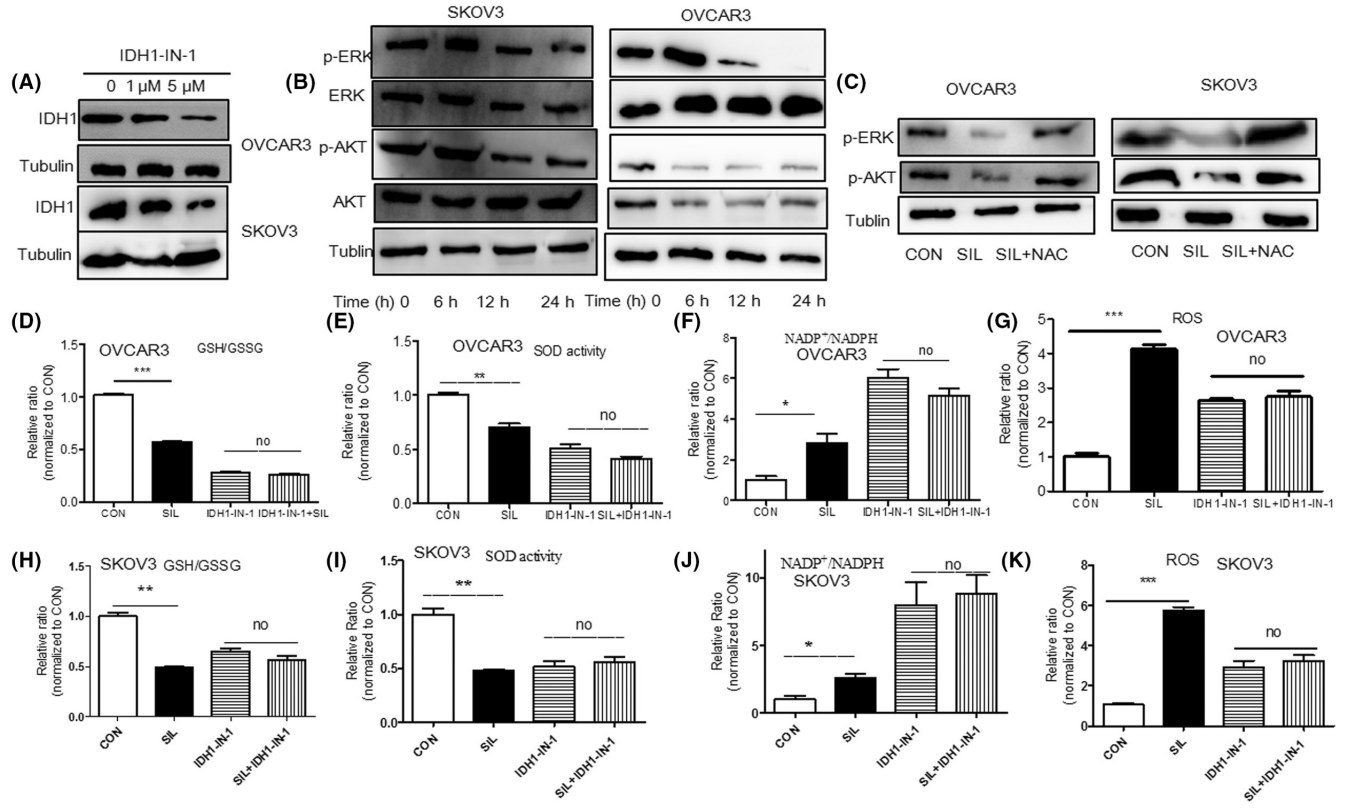

FIGURE 6 Effect of SIL on the ERK and Akt. (A) Protein levels of IDH1 were determined in cell lysates from cells treated with solvent control or IDH1-IN-1 (1 μM or 5 μM) for 24 h by performing immunoblotting. (B) OVCAR3 and SKOV3 cells were exposed to 100 μM SIL for various times. Expression of p-ERK, p-Akt, ERK, and AKT was evaluated by western blot analysis. (C) OVCAR3 and SKOV3 cells were exposed to 100 μM SIL in the presence or absence of 5 mM NAC for 24 h. Expression of p-ERK and p-Akt was evaluated by western blot analysis. (D, F, H, J) Ratios of GSH/GSSG and $NADP^+$/NADPH in cells ($n = 5$). (E, I) The activity of SOD in cells ($n = 5$). (G, K) Cells were loaded with DCFH-DA for 1 h and after treatment with 100 μM SIL for 24 h. DCF fluorescence intensity was measured by flow cytometry. Statistical analysis: Student's *t*-test. Error bars represent SEM, and $P < 0.05$ was considered statistically significant. $^*P < 0.05$, $^{**}P < 0.01$, $^{***}P < 0.001$, All experiments were repeated three times

The ratios of GSH/GSSG and $NADP^+$/NADPH were both significantly increased, whereas SOD activity was decreased after SIL treatment compared with the control, but no change was observed for IDH1-IN-1 between the presence or absence of SIL (Figure 6D–K). These results indicated that SIL inhibited the phosphorylation of ERK and AKt, and disrupted the balance between oxidative and reducing substances.

3.7 | SIL inhibits the growth of OVCAR3 cells in axenotransplantation mice model

To determine the antineoplastic effect of SIL in vivo, an OVCAR-3 xenograft was created in BALB/c nude mice by subcutaneous injection. The animals were then given SIL or saline by oral gavage daily. Because previous research had shown that doses of 100–200 mg/kg of SIL play an anti-tumor role in the animal model of human bladder cancer and glioblastoma,[18,19] combined with previous pre-experiment results, we chose a dose of 100 mg/kg body weight. Following 6 weeks of treatment, the size of the tumor was assessed postmortem. The tumor volume and tumor weight were significantly smaller in the SIL-treated mice than in mice receiving saline treatment, except for transfection of the sh-IDH1 lentiviral vector (Figure 7A–C). IDH1-knockdown OVCAR3 cells significantly suppressed tumor growth compared with parent OVCAR3 cells, IDH1-overexpressing OVCAR3 cells significantly enhance tumor growth compared with parent cells (Figure 7D). Interestingly, there was no change in the body weight of the mice (Figure S3). The latter displayed more mitotic signs and an increased nucleoplasmic ratio compared with the SIL-treated animals (Figure 7E). For analysis of the collected tumor-forming tissues, IDH1 expression was knocked down after transfection with the sh-IDH1 lentiviral vector, and there was overexpression after transfection with the OV-IDH1 lentiviral vector (Figure 7F). All these results suggested that IDH1 expression was inhibited as a result of the treatment, which could control the growth of cancer tissue to some extent (Figure 8).

4 | DISCUSSION

SIL is a natural polyphenolic compound with anti-neoplasmic and anti-diabetic activity.[20,21] We observed that treatment of an ovarian cancer cell line with SIL increased ROS generation. This SIL-induced ROS generation coincided with binding to IDH1 and decreased its activity by altering its phosphorylation levels. NADPH is a matter reductant needed at high demand in tumor cells to fuel the synthesis of lipids and antioxidants; several studies have shown that IDH1 is an important source of NADPH in cytoplasm.[22,23] These studies,

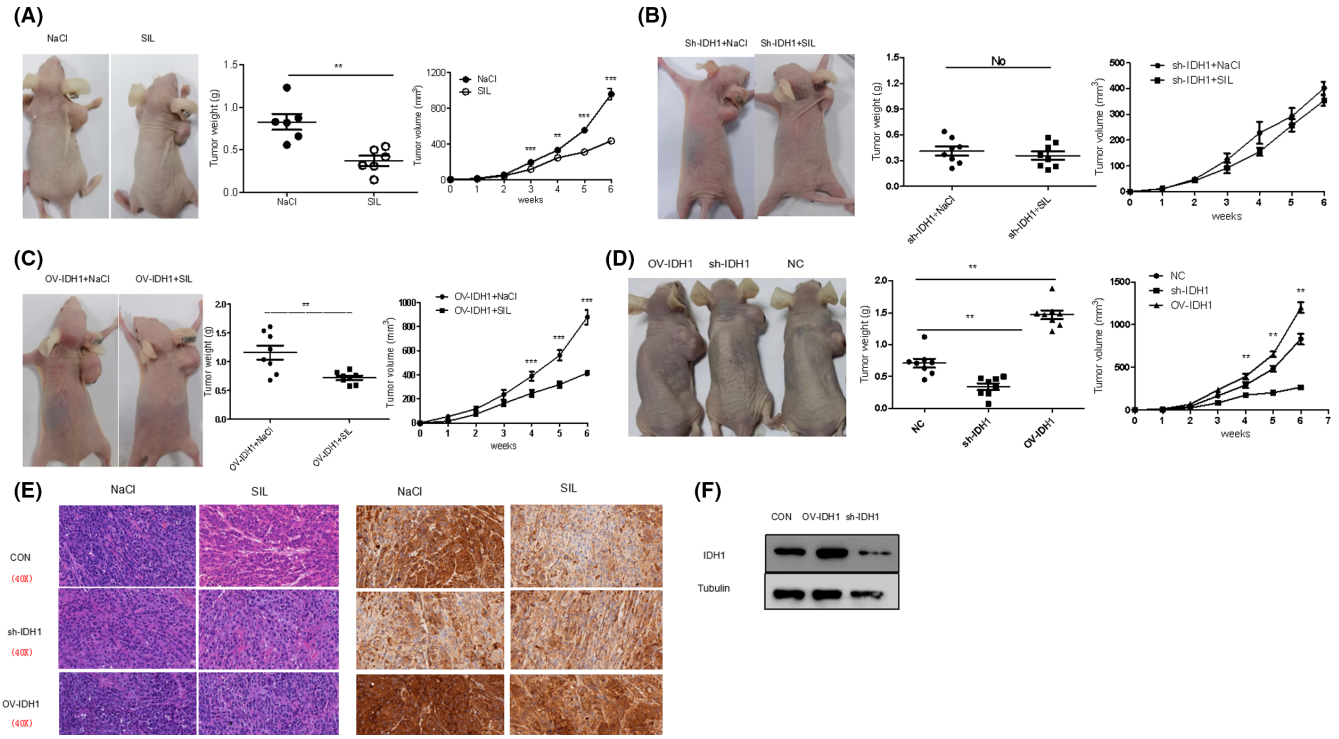

FIGURE 7 SIL inhibits the growth of OVCAR3 cells in a xenotransplantation mice model. Cells (2×10^6) were injected subcutaneously into the right hind leg of 4-week-old female nude mice. After injection, SIL (100 mg/kg) in 10 μl of saline or with 100 μl of saline (vehicle) was administered by oral gavage daily. The tumor volume was recorded weekly throughout experiments. After 6 weeks, the tumors were excised and tumor volume was calculated using the following equation: tumor volume (mm^3) = (length × $width^2$)×π/6. (A–D) Tumor volume and weight. (E) Immunohistochemical analysis of the expression IDH1 in the tumor tissues. (F) Western blot analysis of IDH1 expression in the tumor tissues. Statistical analysis: Student's *t*-test. Error bars represent SEM, and $P<0.05$ was considered statistically significant. $^{**}P<0.01$. All experiments were repeated three times.

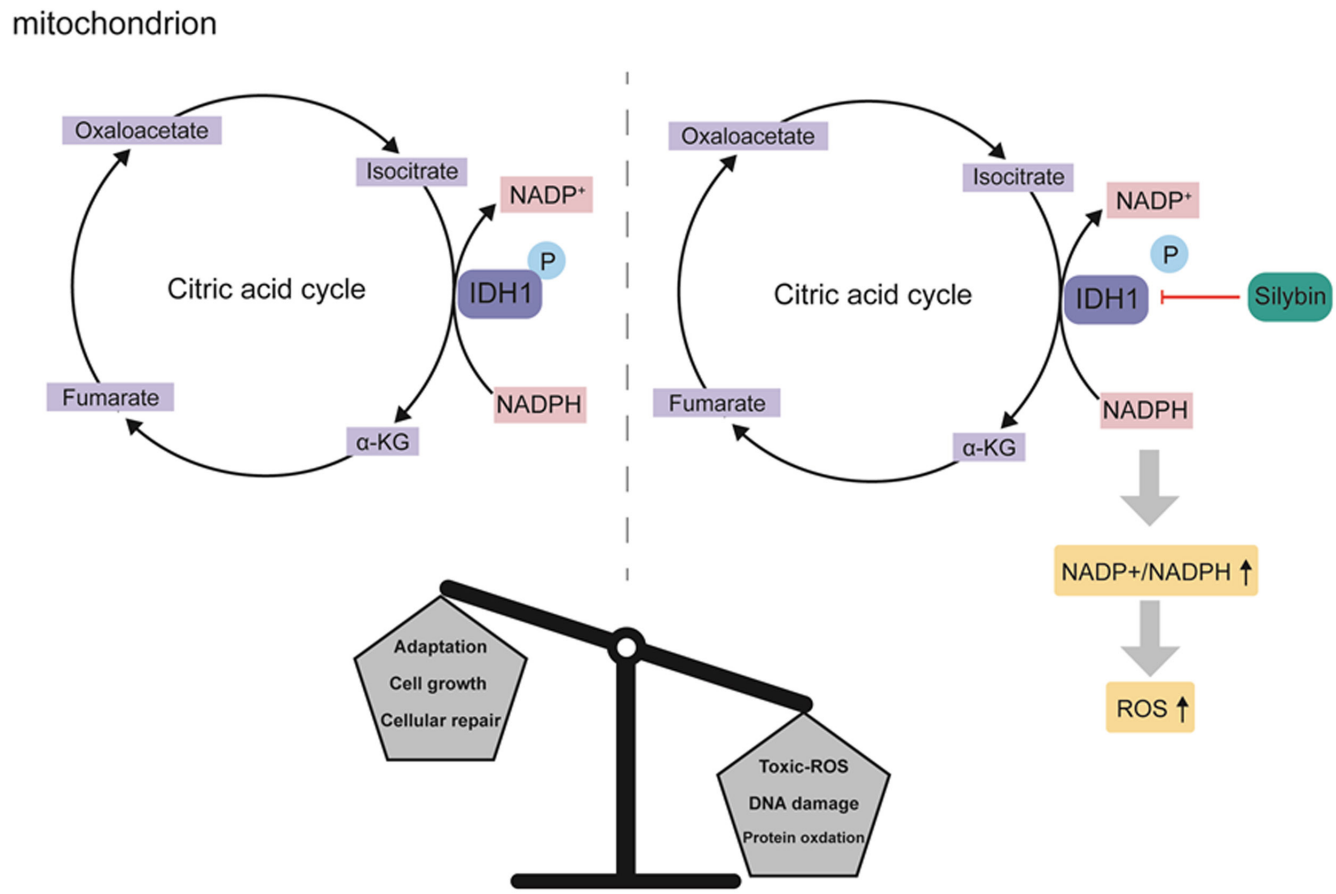

FIGURE 8 Mechanism of Silybin suppresses ovarian cancer cell proliferation

together with our observation that SIL can increase the $NADP^+$/NADPH ratio (Figure 6F,J), suggested that IDH1-generated cytoplasmic NADPH is important for redox homeostasis to accelerate tumor growth and survival. The molecular mechanism for the toxicity of SIL toward tumor cells takes place via the IDH1/NADPH/ROS cascade.

ROS, produced by various biochemical and physiological oxidative processes in the body, are associated with numerous physiological and pathophysiological processes.[24] ROS can induce the activation of AKt and ERK; conversely it has also been reported that ROS can trigger the downregulation of the ERK and Akt pathways.[25,26] ROS play the role of signaling molecules in cancer, promoting abnormal cell growth and metabolic disorders, and can lead to a differentiation blockade.[27,28] Elevated ROS levels can increase glucose metabolism.[29,30] Nevertheless, ROS toxicity levels in cancer have anti-tumor effects, leading to increased irreparable DNA damage, genomic instability, and tumor cell death.[31,32] When the TCA cycle is dampened, intracellular ROS levels are increased, which reduces ATP production, potentially reducing cell proliferation.[14] Aberrant metabolism, also called metabolism reprogramming, is a common characteristic of cancer cells; changes in cancer cell metabolism can affect the response to many chemotherapy treatments.[33,34] Ovarian cancer is characterized by tumor cells displaying high glycolysis rates; the involved enzymes present probable candidates for specific treatment targets.[2,35,36] In addition to glucose, proliferating cancer cells also rely on glutamine.[37] For this reason, targeting enzymes involved in glutamine production and associated ROS generation may provide a novel approach for treatment of ovarian cancer.

SIL abolishes the decrease of various antioxidants.[38] It also regulates glucose uptake in adipocytes by obstructing insulin-dependent glucose transporter 4 (GLUT4).[39] Here, we report that SIL had no significant effect on ECAR. However, the oxygen consumption rate, ATP production, and basal respiration were all reduced in SIL-treated OVACR3 cells (Figure 2A,B,E). In addition, SIL not only blocked the generation of succinate from glutamate, but also obviously interfered with both glutamine catabolism and reductive carboxylation, which are catalyzed by IDHs and glutamate dehydrogenase, as the latter catalyzes the reversible oxidative deamination of glutamate to α-KG.

Inhibition of IDH activity may be an important method, even in cancers in which IDH mutations are not involved.[12] The drug AG-120 has been approved by the United States Food and Drug Administration to treat cancers with IDH mutations.[40] Our study clearly demonstrates that SIL can bind to IDH1 in cells; this report is the first to our knowledge describing that activity. Our interpretation was corroborated using the DARTS method, which can detect a protein target of a drug, as binding of the drug and protein protects the latter from degradation.[41,42] Phosphorylation is a very common

strategy in the cell to regulate protein activity or expression, and approximately one-third of proteins are typically phosphorylated. Chen and colleagues demonstrated phosphorylation of IDH1 monomers, which promotes the formation of dimers that display enhanced binding toward the substrates isocitrate and α-ketoglutarate.[43] Our results showed that IDH1 phosphorylation markedly decreased as a result of SIL treatment.

As described by Calvert and colleagues, IDH1 has a higher maximal enzymatic activity than other enzymes that produce NADPH in glioblastoma tissue. It is the most difference in the expression NADPH-producing enzyme in glioblastoma compared with normal group.[44] These studies, together with the observations described here that identified increased citrate concentrations in SIL-treated cells, indicate that the NADPH produced by IDH1 is the key and possible rate limiting factor for maintaining ROS homeostasis, in agreement with the interpretation by others.

In healthy tissue, cells have an adequate means to remove excessive ROS. Tumor cells express increased levels of antioxidants (GSH, NADPH and SOD) to clear spare ROS, whereas they maintain tumor-promoting signaling activities. Our results showed that SOD activity, as well as the ratios of GSH/GSSG and $NADP^+$/NADPH, all dramatically declined with increasing ROS levels, resulting in toxic ROS concentrations. This is consistent with a previous report that described how the toxicity of the sensitizer Rose Bengal in the acute promyelocytic leukemia (AML) cell line HL-60 was enhanced by knockdown IDH1, which resulted in decreased levels of GSH and NADPH and increased ROS production.[45] Altogether, we provide evidence that suggests a potential for SIL for suppressing tumor proliferation by interfering with the redox balance and we consider SIL a novel candidate for the treatment of ovarian cancer.

AUTHOR CONTRIBUTIONS

J.Y. and Q.L. designed the research; J.Y. and Z.W. analyzed the data; and J.Y. and Z.W. wrote the paper; Z.W., S.Y. and H.F. performed the experiments; C.Z. purchased the reagents and materials; X.D. and X.Z. provided guidance on experimental technology; X.L. and L.Z. acquired the data. All authors read and approved the final manuscript.

CONFLICT OF INTEREST

The authors have no conflict of interest.

DATA AVAILABILITY STATEMENT

The data supporting the findings of this study are available from the corresponding author upon reasonable request.

ETHICS STATEMENT

Approval of the research protocol by an Institutional Reviewer Board: The study protocol was approved by the Investigation Ethical Committee of Shunde Hospital of Southern Medical University. Informed Consent: All patients or their guardians were given and accepted informed consent. Registry and the Registration No. of the study/trial: The study protocol was approved by the Investigation Ethical Committee of Shunde Hospital of Southern Medical University (registration no. 20191108). Animal Studies: All experiments were carried out in accordance with the National Institutes of Health (NIH) Guidelines for the Care and Use of Laboratory Animals and approved by the Southern Medical University Animal Administration Committee.

ORCID

Zibo Wei https://orcid.org/0000-0002-5306-7407
Haipeng Feng https://orcid.org/0000-0003-3412-7264
Xiaokang Zeng https://orcid.org/0000-0002-6531-2502
Jie Yao https://orcid.org/0000-0002-8935-0722

REFERENCES

1. Torre LA, Trabert B, DeSantis CE, et al. Ovarian cancer statistics, 2018. *CA Cancer J Clin*. 2018;68:284-296.
2. Dahl ES, Buj R, Leon KE, et al. Targeting IDH1 as a prosenescent therapy in high-grade serous ovarian cancer. *Mol Cancer Res*. 2019;17:1710-1720.
3. Crocenz FA, Roma MG. Silymarin as a new hepatoprotective agent in experimental cholestasis: new possibilities for an ancient medication. *Curr Med Chem*. 2006;13:1055-1074.
4. Seidlová-Wuttke D, Becker T, Christoffel V, Jarry H, Wuttke W. Silymarin is a selective estrogen receptor β (ERβ) agonist and has estrogenic effects in the metaphysis of the femur but no or anti-estrogenic effects in the uterus of ovariectomized (ovx) rats. *J Steroid Biochem Mol Biol*. 2003;86:179-188.
5. Plíšková M, Vondráček J, Křen V, et al. Effects of silymarin flavonolignans and synthetic silybin derivatives on estrogen and aryl hydrocarbon receptor activation. *Toxicology*. 2005;215:80-89.
6. Yang H, Xia G, Tan C, Xu X, Shang Y, Fu X. A novel approach for the efficient extraction of silybin from milk thistle fruits. *Pharmacogn Mag*. 2014;10:536.
7. Nejati-Koshki K, Zarghami N, Pourhassan-Moghaddam M, et al. Inhibition of leptin gene expression and secretion by silibinin: possible role of estrogen receptors. *Cytotechnology*. 2012;64:719-726.
8. Cho HJ, Suh DS, Moon SH, et al. Silibinin inhibits tumor growth through downregulation of extracellular signal-regulated kinase and Akt in vitro and in vivo in human ovarian cancer cells. *J Agric Food Chem*. 2013;61:4089-4096.
9. Moloney JN, Cotter TG. ROS signalling in the biology of cancer. *Semin Cell Dev Biol*. 2018;80:50-64.
10. Detaille D, Sanchez C, Sanz N, Lopez-Novoa JM, Leverve X, El-Mir M-Y. Interrelation between the inhibition of glycolytic flux by silibinin and the lowering of mitochondrial ROS production in perifused rat hepatocytes. *Life Sci*. 2008;82:1070-1076.
11. Zhao S, Lin Y, Xu W, et al. Glioma-derived mutations in IDH1 dominantly inhibit IDH1 catalytic activity and induce HIF-1. *Science*. 2009;324:261-265.
12. Bergaggio E, Piva R. Wild-type IDH enzymes as actionable targets for cancer therapy. *Cancer*. 2019;11:563.
13. Dang L, White DW, Gross S, et al. Cancer-associated IDH1 mutations produce 2-hydroxyglutarate. *Nature*. 2009;462:739-744.
14. Calvert AE, Chalastanis A, Wu Y, et al. Cancer-associated IDH1 promotes growth and resistance to targeted therapies in the absence of mutation. *Cell Rep*. 2017;19:1858-1873.
15. Hu Y, Zhang M, Tian N, et al. The antibiotic clofoctol suppresses glioma stem cell proliferation by activating KLF13. *J Clin Invest*. 2019;129:3072-3085.
16. Ye S, Xu P, Huang M, et al. The heterocyclic compound tempol inhibits the growth of cancer cells by interfering with glutamine metabolism. *Cell Death Dis*. 2020;11:312.

17. DeBerardinis RJ, Mancuso A, Daikhin E, et al. Beyond aerobic glycolysis: transformed cells can engage in glutamine metabolism that exceeds the requirement for protein and nucleotide synthesis. *Proc Natl Acad Sci*. 2007;104:19345-19350.
18. Singh RP, Tyagi A, Sharma G, Mohan S, Agarwal R. Oral silibinin inhibits in vivo human bladder tumor xenograft growth involving down-regulation of survivin. *Clin Cancer Res*. 2008;14:300-308.
19. Kim KW, Choi CH, Kim TH, Kwon CH, Woo JS, Kim YK. Silibinin inhibits glioma cell proliferation via Ca2+/ROS/MAPK-dependent mechanism in vitro and glioma tumor growth in vivo. *Neurochem Res*. 2009;34:1479-1490.
20. Delmas D, Xiao J, Vejux A, Aires V. Silymarin and cancer: A dual strategy in both in chemoprevention and chemosensitivity. *Molecules*. 2020;25(9):2009.
21. Si L, Fu J, Liu W, et al. Silibinin inhibits migration and invasion of breast cancer MDA-MB-231 cells through induction of mitochondrial fusion. *Mol Cell Biochem*. 2020;463:189-201.
22. Wahl DR, Dresser J, Wilder-Romans K, et al. Glioblastoma therapy can be augmented by targeting IDH1-mediated NADPH biosynthesis. *Cancer Res*. 2017;77:960-970.
23. Itsumi M, Inoue S, Elia AJ, et al. Idh1 protects murine hepatocytes from endotoxin-induced oxidative stress by regulating the intracellular NADP(+)/NADPH ratio. *Cell Death Differ*. 2015;22:1837-1845.
24. Giorgio M, Trinel M, Migliaccio E, Pelicci PG. Hydrogen peroxide: A metabolic by-product or a common mediator of ageing signals. *Nat Rev Mol Cell Biol*. 2007;8(9):722-728.
25. Su X, Shen Z, Yang Q, et al. Vitamin C kills thyroid cancer cells through ROS-dependent inhibition of MAPK/ERK and PI3K/AKT pathways via distinct mechanisms. *Theranostics*. 2019;9:4461-4473.
26. Sharma P, Caldwell TS, Rivera MN, Gullapalli RR. Cadmium exposure activates Akt/ERK signaling and pro-inflammatory COX-2 expression in human gallbladder epithelial cells via a ROS dependent mechanism. *Toxicology In Vitro: An International Journal Published in Association with BIBRA*. 2020;67:104912.
27. Moloney JN, Stanicka J, Cotter TG. Subcellular localization of the FLT3-ITD oncogene plays a significant role in the production of NOX- and p22(phox)-derived reactive oxygen species in acute myeloid leukemia. *Leuk Res*. 2017;52:34-42.
28. Sabharwal SS, Schumacker PT. Mitochondrial ROS in cancer: initiators, amplifiers or an Achilles' heel? *Nat Rev Cancer*. 2014;14:709-721.
29. Vander Heiden MG, Cantley LC, Thompson CB. Understanding the Warburg effect: the metabolic requirements of cell proliferation. *Science*. 2009;324:1029-1033.
30. Levine AJ, Puzio-Kuter AM. The control of the metabolic switch in cancers by oncogenes and tumor suppressor genes. *Science*. 2010;330:1340-1344.
31. Nogueira V, Park Y, Chen CC, et al. Akt determines replicative senescence and oxidative or oncogenic premature senescence and sensitizes cells to oxidative apoptosis. *Cancer Cell*. 2008;14:458-470.
32. Dickinson BC, Chang CJ. Chemistry and biology of reactive oxygen species in signaling or stress responses. *Nat Chem Biol*. 2011;7:504-511.
33. Zangar R. Mechanisms that regulate production of reactive oxygen species by cytochrome P450. *Toxicol Appl Pharmacol*. 2004;199:316-331.
34. Ye D, Guan K-L, Xiong Y. Metabolism, activity, and targeting of D- and L-2-hydroxyglutarates. *Trends in Cancer*. 2018;4:151-165.
35. Xintaropoulou C, Ward C, Wise A, et al. Expression of glycolytic enzymes in ovarian cancers and evaluation of the glycolytic pathway as a strategy for ovarian cancer treatment. *BMC Cancer*. 2018;18:636.
36. Berek JS, Kehoe ST, Kumar L, Friedlander M. Cancer of the ovary, fallopian tube, and peritoneum. *Int J Gynecol Obstet*. 2018;143:59-78.
37. DeBerardinis RJ, Cheng T. Q's next: the diverse functions of glutamine in metabolism, cell biology and cancer. *Oncogene*. 2009;29:313-324.
38. Loguercio C. Silybin and the liver: from basic research to clinical practice. *World J Gastroenterol*. 2011;17:2288-2301.
39. Pignatelli P, Carnevale R, Menichelli D. Silybin and metabolic disorders. *Intern Emerg Med*. 2018;14:1-3.
40. Kim ES. Enasidenib: first global approval. *Drugs*. 2017;77:1705-1711.
41. Derry MM, Somasagara R, Raina K, et al. Target identification of grape seed extract in colorectal cancer using drug affinity responsive target stability (DARTS) technique: role of endoplasmic reticulum stress response proteins. *Curr Cancer Drug Targets*. 2014;14:323-336.
42. Pai MY, Lomenick B, Hwang H, et al. Drug affinity responsive target stability (DARTS) for small-molecule target identification. *Methods Mol Biol*. 2015;1263:287-298.
43. Chen D, Xia S, Wang M, et al. Mutant and wild-type isocitrate dehydrogenase 1 share enhancing mechanisms involving distinct tyrosine kinase cascades in cancer. *Cancer Discov*. 2019;9:756-777.
44. Bleeker FE, Atai NA, Lamba S, et al. The prognostic IDH1 (R132) mutation is associated with reduced NADP+-dependent IDH activity in glioblastoma. *Acta Neuropathol*. 2010;119:487-494.
45. Kim SY, Lee SM, Tak JK, Choi KS, Kwon TK, Park J-W. Regulation of singlet oxygen-induced apoptosis by cytosolic NADP+-dependent isocitrate dehydrogenase. *Mol Cell Biochem*. 2007;302:27-34.

SUPPORTING INFORMATION

Additional supporting information can be found online in the Supporting Information section at the end of this article.

How to cite this article: Wei Z, Ye S, Feng H, et al.. Silybin suppresses ovarian cancer cell proliferation by inhibiting isocitrate dehydrogenase 1 activity. *Cancer Sci*. 2022;113:3032-3043. doi: 10.1111/cas.15470